Journal of Alloys and Compounds 488 (2009) 211–216

Contents lists available at ScienceDirect

Journal of Alloys and Compounds

journal homepage: www.elsevier.com/locate/jallcom

Dielectric and piezoelectric studies of perovskite–tungsten bronze structured $(1-x)$PLZT–xPBBiN nanoceramic composites by high-energy mechanical activation technique

Koduri Ramam[a,*], Marta Lopez[a], K. Chandramouli[b]

[a] Departmento de Ingenieria de Materials, (DIMAT), Facultad de Ingenieria, Universidad de Concepcion, Concepcion, Chile
[b] Solid State Physics and Materials Research Laboratory, Department of Physics, Andhra University, Visakhapatnam, India

ARTICLE INFO

Article history:
Received 21 July 2009
Received in revised form 10 August 2009
Accepted 10 August 2009
Available online 24 August 2009

Keywords:
Ferroelectrics
X-ray diffraction
Dielectric response
Mechanical activation
Piezoelectricity

ABSTRACT

Polycrystalline $(1-x)$PLZT–xPBBiN ferroelectric complex ceramic nanocomposites were synthesized through high-energy mechanical activation technique. It is found that milling time has a significant impact on the phase formation, particle size and grain growth. The optimized compositions were subjected to XRD, SEM, dielectric and piezoelectric studies. Powder X-ray diffraction studies revealed that the nanocomposites consisted of both perovskite (tetragonal) and tungsten bronze (orthorhombic) structures whilst pure PLZT showed perovskite structure and pure PBBN showed tungsten bronze structure. As the PBBN content increased, the in situ prepared perovskite and tungsten bronze nanocomposites revealed a bi-phase formation. It is worth mentioning that crack-free nanoceramic composites were obtained. The maximum dielectric constant (ε_{RT} = 2509), piezoelectric planar coupling coefficient (k_p = 0.584) and the piezoelectric charge coefficient (d_{33} = 596 pC/N) were observed for x = 0.6 nanoceramic composite. It has been observed that the dielectric and piezoelectric constants increased gradually with increasing x up to 0.6 and was found optimum, which could be ideal for electromechanical and energy harvesting applications.

1. Introduction

Tungsten bronzes M_xWO_3 (M = alkali atoms) have long been the subject of investigations for their interesting structural, electronic, and electrooptic properties [1,2]. The word "bronze" has been applied to non-stoichiometric crystalline of transitional metal oxide, especially ternary (tetragonal tungsten bronze (TTB), hexagonal tungsten bronze (HTB) and intergrowth tungsten bronze (ITB)) systems. The crystalline structure of tungsten trioxide is based on corner-shared W—O octahedra [3]. Ferroelectric compositions of the tungsten bronze-type can be represented by the chemical formula $(A1)_2(A2)_4(C)_4(B1)_2(B2)_8O_{30}$, where positions A1, A2, B1, B2 and C will be filled by different valency cations or may be partially empty. In tungsten bronze niobates, B1 and B2 are filled by Nb^{5+}, A1, A2 and C could be filled by alkali and alkaline earth metal ions. One of the important tungsten bronze relaxor ferroelectrics is lead barium niobate $Pb_xBa_{1-x}Nb_2O_6$ (PBN) solid solution because of its morphotrophic phase boundary (MPB) and its potential applications [4,5]. The tungsten bronze crystal structures especially the Barium Strontium Niobate ($Ba_{0.27}Sr_{0.75}Nb_2O_{5.78}$) with T_c = 348 ± K which crystallizes in the tetragonal system have been discussed [6]. Another in-depth study of ferroelectric tungsten bronze-type crystal structures of $Ba_{(4+x)}Na_{(2-2x)}Nb_{10}O_{30}$ with a Curie temperature of 833 K which crystallizes in the orthorhombic system have been reported [7].

At the same time, the electromechanical properties of well known perovskite $Pb(Zr,Ti)O_3$ ceramics can be improved by additives [8]. The donor ions like La^{3+} incorporated into the PZT lattice can be tailored for specific desired properties, such as dielectric, ferroelectric and piezoelectric properties for specific applications. The lanthanum-modified PZT known as PLZT $[(Pb^{2+},La^{3+})(Zr^{4+},Ti^{4+})O_3]$ near morphotrophic phase boundary (MPB with Zr/Ti ratio ≈ 52/48) has been extensively studied and tailored for specific properties, since these compositions contribute better ferroelectric and piezoelectric properties [9]. The conventional solid state reaction route to synthesize tungsten bronze involves mixing of oxides in stoichiometric ratios, calcination and sintering process at elevated temperatures ≈ 1200–1300 °C [10,11]. The influence of $SrBi_2Nb_2O_9$ (SBN) on dielectric and ferroelectric properties of (PLZT) ceramics was systematically investigated [12]. La^{3+}-doped and undoped PBN56 ceramics were studied in order to investigate the composition range for the formation of the orthorhombic phase caused by the La^{3+} doping [13]. However, the concern is about the undesirable lead loss, which influences structural and functional properties.

* Corresponding author. Tel.: +56 41 2203369; fax: +56 41 2203391.
E-mail address: ramamk@udec.cl (K. Ramam).

0925-8388/$ – see front matter © 2009 Elsevier B.V. All rights reserved.
doi:10.1016/j.jallcom.2009.08.082

To overcome this limitation, it is certainly essential to have a process, where lead loss can be restricted by processing at low temperatures. Nanocrystalline materials are of great interest both from technology and applications viewpoint. Since properties of nanocrystalline materials are synthesis/process dependent, much attention is therefore, required towards the process optimization of nanomaterials.

It is well known that perovskite materials have been extensively investigated for several tailored properties [14]. In general, there are different techniques that have been explored for the synthesis route but the mechanical activation route has extremely been limited to understand the effect of PLZT–PBBiN composites on several tailored characteristics. Mechanical activation process can also be termed as high-energy ball milling, high-energy mechanical milling, high-energy mechanical activation or mechanical alloying, etc. In this study, we report the structural and functional properties of binary structured $(1-x)$PLZT–xPBBiN composites synthesized through mechanical activation technique.

2. Experimental procedure

2.1. Synthesis of $(1-x)$PLZT–xPBBiN nanocomposites

Analytical reagent grade (99.99% purity) starting materials (PbO, La_2O_3, ZrO_2, TiO_2, $BaCO_3$, Bi_2O_3 and Nb_2O_5 (Sigma–Aldrich, USA) were subjected to high-energy mechanical activation milling to obtain PLZT–PBBN composites with the stoichiometric formula $(1-x)[Pb_{0.988}La_{0.012}(Zr_{0.53}Ti_{0.47})_{0.997}O_3]$–$x[Pb_{0.59}Ba_{0.38}Bi_{0.02}Nb_2O_6]$. Please refer Table 1. The synthesis was carried out using Fritsch Pulverisette 5 ball milling system. Appropriate amounts of the constituent oxides as per the stoichiometric compositions were mixed together and milled in a 250 ml agate bowl with high wear resistant Zirconia grinding media. The balls were 3 mm in diameter, and the ball to powder ratio was 10:1 and milling was carried out in toluene medium. Milling was done at a speed of 150, 200, 250 and 300 rpm for 20, 25, 30, 35 and 40 h. The milling was stopped for 5 min after every 30 min of milling to cool down the system. The milled powders were calcined at 850 °C for 2 h. Calcined batch powders were ground for crushing agglomerates and 5 wt% PVA binder was added, and subsequently powders were pressed into pellets of 12 mm in diameter and 2 mm thickness, using a steel die and uniaxial hydraulic cold pressing with pressures of 700–900 kg/cm^2. The green bodies were sintered at 1025 °C for 2 h and samples were allowed to cool in the furnace.

2.2. Structural characterization of $(1-x)$PLZT–xPBBiN nanocomposites

The phase formation in the nanocomposites were analyzed by powder X-ray diffraction (XRD) technique (Philips X-ray diffractometer PW-1710) using CuK_α radiation with Ni filter at room temperature and a step scan from $2\theta = 20$–80°. JEOL JSM 840A scanning electron microscopy was used to analyze microstructure of polished, etched and fractured ceramic surfaces. The morphology of nanoparticles was observed by JEOL TEM 1200 transmission electron microscope. Densities of sintered batch samples were measured by Archimedes method. Polished and silver electroded specimens were characterized for temperature dependent dielectric response by using HP 4192A impedance analyzer and a programmable furnace. The electroded specimens were poled in silicon oil bath at 100 °C by applying a dc field of 20 kV/cm. After 24 h ageing, the poled specimens were characterized for piezoelectric studies. The piezoelectric charge coefficient (d_{33}) was characterized by using a Berlincourt piezo-d-meter. The piezoelectric planar coupling coefficient (k_p) was characterized through resonance and anti-resonance technique by using a 4192A HP impedance analyzer.

3. Results and discussion

3.1. Optimization of $(1-x)$PLZT–xPBBiN nanocomposites

The evolution of the phase formation from oxide precursors caused by high-energy mechanical activation process is milling speed and time dependent. We had taken $x = 0.2$ composition in this series which was milled at a speed of 150, 200, 250 and 300 rpm for 20, 25, 30, 35 and 40 h and milled powders were subjected to XRD for optimization. The milling was stopped for 5 min after every 30 min of milling to cool down the system. It is found that milling time has a significant impact on the phase formation. It is observed for $x = 0.2$ composition in $(1-x)$PLZT–xPBBiN, 250 rpm milling speed for 25 h had shown best results than other milling

Table 1
$(1-x)$PLZT–xPBBiN nanoceramic composites.

sComposition	Formulae		
General formula – $(1-x)$PLZT–$_x$PBBiN	$(1-x)[Pb_{1-w}La_w][(Zr_zTi_{1-z})_{1-(w/4)}]O_3 - x[Pb_{(1-k-3z/2)}Ba_kBi_zNb_2O_6]$		
Stoichiometric Formula	$(1-x)[(Pb_{0.988}La_{0.012})(Zr_{0.53}Ti_{0.47})_{0.997}O_3] - x[Pb_{0.59}Ba_{0.38}Bi_{0.02}Nb_2O_6]$		
	Where $x = 0, 0.2, 0.4, 0.6, 0.8, 1$, Ba = $k = 38$ mol%, La = $w = 1.2$ mol%, and Bi = $z = 2$ mol%		
Compositions	Reactants		Products
PLZT	$0.988PbO + 0.006La_2O_3 + 0.528410ZrO_2 + 0.468590TiO_2$	→	$[Pb_{0.988}La_{0.012}(Zr_{0.53}Ti_{0.47})_{0.997}O_3]$
0.8PLZT–0.2PBBiN:	$0.8[0.988PbO + 0.006La_2O_3 + 0.528410ZrO_2 + 0.468590TiO_2] + 0.2[0.59PbO + 0.38BaCO_3 + 0.01Bi_2O_3 + Nb_2O_5]$	→	$0.8[Pb_{0.988}La_{0.012}(Zr_{0.53}Ti_{0.47})_{0.997}O_3] - 0.2[Pb_{0.59}Ba_{0.38}Bi_{0.02}Nb_2O_6] + 0.076CO_2\uparrow$
0.6PLZT–0.4PBBiN:	$0.6[0.988PbO + 0.006La_2O_3 + 0.528410ZrO_2 + 0.468590TiO_2] + 0.4[0.59PbO + 0.38BaCO_3 + 0.01Bi_2O_3 + Nb_2O_5]$	→	$0.6[Pb_{0.988}La_{0.012}(Zr_{0.53}Ti_{0.47})_{0.997}O_3] - 0.4[Pb_{0.59}Ba_{0.38}Bi_{0.02}Nb_2O_6] + 0.152CO_2\uparrow$
0.4PLZT–0.6PBBiN:	$0.4[0.988PbO + 0.006La_2O_3 + 0.528410ZrO_2 + 0.468590TiO_2] + 0.6[0.59PbO + 0.38BaCO_3 + 0.01Bi_2O_3 + Nb_2O_5]$	→	$0.4[Pb_{0.988}La_{0.012}(Zr_{0.53}Ti_{0.47})_{0.997}O_3] - 0.6[Pb_{0.59}Ba_{0.38}Bi_{0.02}Nb_2O_6] + 0.228CO_2\uparrow$
0.2PLZT–0.8PBBiN:	$0.2[0.988PbO + 0.006La_2O_3 + 0.528410ZrO_2 + 0.468590TiO_2] + 0.8[0.59PbO + 0.38BaCO_3 + 0.01Bi_2O_3 + Nb_2O_5]$	→	$0.2[Pb_{0.988}La_{0.012}(Zr_{0.53}Ti_{0.47})_{0.997}O_3] - 0.8[Pb_{0.59}Ba_{0.38}Bi_{0.02}Nb_2O_6] + 0.304CO_2\uparrow$
PBBiN:	$[0.59PbO + 0.38BaCO_3 + 0.01Bi_2O_3 + Nb_2O_5]$	→	$[Pb_{0.59}Ba_{0.38}Bi_{0.02}Nb_2O_6] + 0.38CO_2\uparrow$

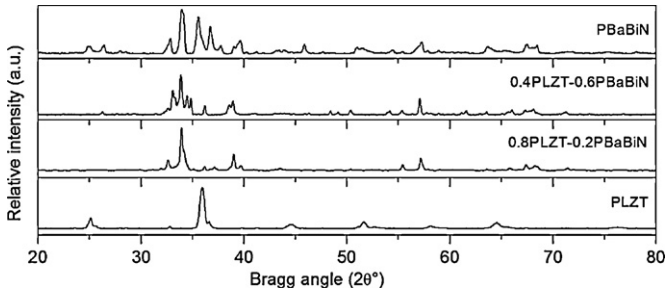

Fig. 1. X-ray diffraction patterns of $(1-x)$PLZT–xPBBiN nanoceramic composites.

speed and hours. Thus, the optimized conditions in this series amongst different milling speed and hours are Fritsch Pulverisette milling process at a speed of 250 rpm for 25 h. The literature survey indicated that PLZT [15], PZT [16] and PBN [17] ceramics have been synthesized separately through high-energy mechanical activation process and to the best knowledge of the author there is no literature on $(1-x)$PLZT–xPBBiN complex ferroelectric nanocomposite system.

3.2. X-ray diffraction patterns of $(1-x)$PLZT–xPBBiN nanocomposites

Fig. 1 indicates powder X-ray diffraction patterns of $(1-x)$PLZT–xPBBiN nanocomposites. Fig. 2 shows powder X-ray diffraction pattern of 0.4PLZT–0.6PBBiN nanoceramic composite with standard diffraction files 29-776-PLZT-Tetragonal and 73-196-PBN-Orthorhombic phases. X-ray diffraction studies of complex composite indicated coexistence of perovskite PLZT (tetragonal) and tungsten bronze PBBiN (orthorhombic) phases whilst pure PLZT showed perovskite tetragonal symmetry and pure PBBN showed orthorhombic tungsten bronze symmetry. As the PBBN content increased, the in situ prepared perovskite and tungsten bronze complex composite revealed a bi-phase formation. It is found from Fig. 1 that the intensities of XRD peaks of the tungsten bronze phase gradually increase with the increase of x throughout the series. This is due to the mixture of crystallization between the two phases, predominantly with tungsten bronze phase as x increased. As we have chosen the compositions near morphotrophic phase boundary (MPB) in both perovskite $1-x$(PLZT) and tungsten bronze x(PBBiN) compounds, the XRD analysis indicated combined phases. However, it is observed that the shifts of the tungsten bronze phase are more than those of perovskite phase due to the variation of PBBiN in the nanoceramic composite. In the literature, it is reported that Barium Strontium Titanate Niobate (BSTN) composite ceramics showed coexistence of perovskite and tungsten bronze phases and the crystal growth rate of the tungsten bronze phase was higher than that of perovskite phase in BSTN composite ceramics as the sintering temperature increased [18]. It is reported that BST and SBN composite ceramics were prepared in which the coexistence of perovskite (BST) and tungsten bronze (SBN) were observed [19]. In our study, as the tungsten bronze content was increased, Ba^{2+} ions substituted Pb^{2+} and influenced the bi-phase formation. Due to the large Ba^{2+} ions (1.61 Å) substituting Pb^{2+} (1.49 Å) ions in two mixed phases, the XRD peaks of the two mixed phases shifted to lower angles of 2θ. Hence, mixture of tetragonal and orthorhombic characteristics has been strongly identified in $x=0.6$ which is illustrated in Fig. 2. However, there is coexistence of both 180° and 90° domains due to the mixed phases. The substitution of Pb^{2+} by Ba^{2+} and Bi^{3+} resulted in chemical homogeneity as evidenced in Fig. 1 which had a profound influence on the structural and functional properties of the composites. In literature, tungsten bronze structured $Ba_2NaNb_5O_{15}$ (BNN) and perovskite structured $BaTiO_3$ (BT) examined as a function

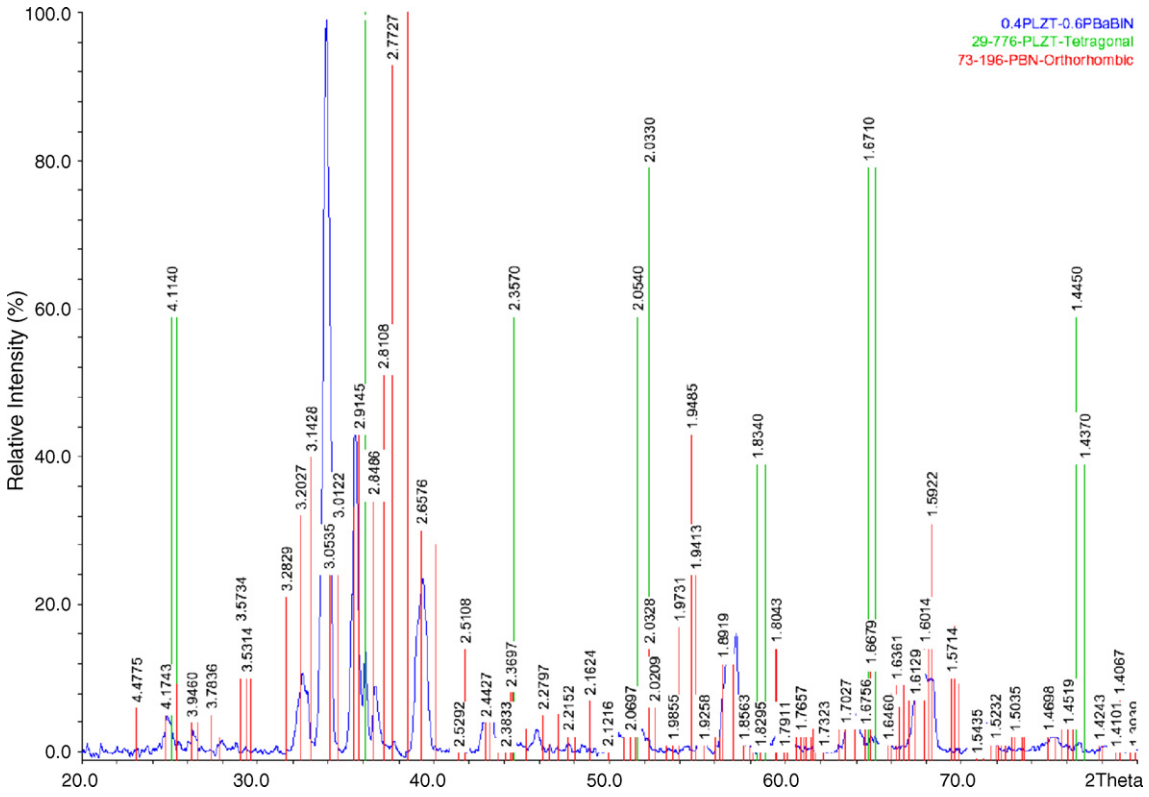

Fig. 2. X-ray diffraction pattern of 0.4PLZT–0.6PBBiN nanoceramic composite.

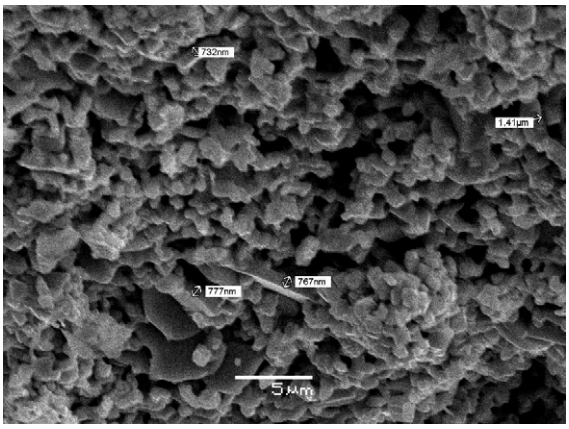

Fig. 3. Scanning electron micrograph of 0.4PLZT–0.6PBBiN nanoceramic composite.

of molar ratio x in $(1-x)Ba_2NaNb_5O_{15}$–$xBaTiO_3$ and coexistence of tungsten bronze and perovskite phases were observed [20]. A similar coexistence of phases has been noticed in our study.

3.3. Structural characterization of $(1-x)$PLZT–xPBBiN nanocomposites

Fig. 3 represents scanning electron micrograph of 0.4PLZT–0.6PBBiN nanoceramic composite. Fig. 4 shows transmission electron micrograph of 0.4PLZT–0.6PBBiN. Microstructural properties revealed homogenous grain growth with well-densified nanoceramic composites. Scanning electron micrograph shows a mixture of semi-spherical grains of perovskite PLZT and elongated grains of tungsten bronze PBBiN. It is worth mentioning that crack-free nanoceramic composites were obtained. It is observed that high-energy mechanical activation route supported in relatively lowering the sintering temperature to 1025 °C and in avoiding lead loss. It was observed that milling speed (250 rpm) and time (25 h) were crucial in obtaining crack-free microstructure supported by surfacial crack-free particles as evidenced in TEM picture. On the contrary, lower milling speed (150 and 200 rpm) and time resulted in micro-particles and higher or prolonged milling speed (300 rpm) and time resulted in surfacial cracks. As x (PBBiN) increased, elongated homogenous grains were evidenced. The well-densified nanocomposites obtained in this study could be due to the volumetric expansion in the lattice in view of the fact that both perovskite and tungsten bronze phases coexist in binary structured nanoceramic composites. The TEM micrograph shows more or less spherical particle morphology and average particle size ranged from 12 to 76 nm. The density of these nanoceramic composites showed an increasing trend from $x=0$ (7.67 g/cm^3) to $x=1$ (7.34 g/cm^3). It was observed in the literature that the density of $0.7BaO–0.3SrO–0.7TiO_2–0.3Nb_2O_5$ (BSTN) composite ceramics had no significant change with the sintering temperature increasing from 1275 to 1300 °C and confirmed that there were porous grains and the variation of measured porosity influenced the density [17]. In our study, the $(1-x)$PLZT–xPBBiN ceramic composite indicated homogenous crystallization and microstructure which could be attributed to the multiple unit cell volume increase and expansion of the crystal structure due to the introduction of PBBiN in PLZT. As x increased, the crystallization increased due to the presence of multiple cations, improving the composite densification and increasing the mobility of the ferroelectric domain wall orientation which resulted in enhanced functional properties. It was observed that $x=0.6$ composition showed well-densified homogenous grains. In literature, PLZT ceramics synthesized via mechanical activation processing revealed the formation of powders on the nano-scale which is comparable with our study [20]. $(1-x)Ba_2NaNb_5O_{15}$–$xBaTiO_3$ generated an abnormal grain growth which is probably due to a liquid phase originated from the second phase [21]. Whereas in our study, SEM picture revealed the intergrowth phases with both intragranular (perovskite PLZT–perovskite PLZT, tungsten bronze–PBBN–tungsten bronze PBBN, respectively) and intergranular (perovskite PLZT–tungsten bronze PBBN) growth.

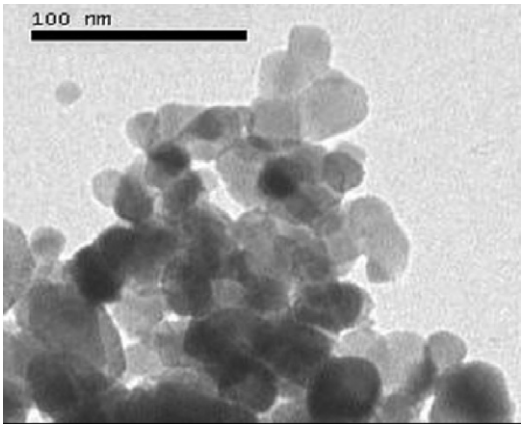

Fig. 4. Transmission electron micrograph of 0.4PLZT–0.6PBBiN.

3.4. Dielectric properties of $(1-x)$PLZT–xPBBiN nanocomposites

Fig. 5 shows the dielectric properties of $(1-x)$PLZT–xPBBiN nanoceramic composites. It is observed that the dielectric constant increased gradually with increasing x (PBBiN) up to 0.6 (optimum) and thereafter decreased which could be due to the multiple cationic arrangements in the nanoceramic composite. The increase in dielectric constant could be attributed to the space charge polarization and presence of two trivalent ions internally substituting the respective lattices, La^{3+} ions in PZT and Bi^{3+} ions in PBN by forming PLZT–PBBiN ceramic composite with both ABO_3 and M_xWO_3 structures in a single composite. Moreover, both the compounds are almost near the MPB range and allow the composite in drastically changing the polarization with temperature, which resulted in increased dielectric constant and dielectric maximum. The dielectric constant at room temperature ($\varepsilon_{RT}=2509$) and dielectric maximum at transition temperature ($\varepsilon_{Tc}=16328$) were found optimum for $x=0.6$ at frequencies of 1 kHz. The dielectric loss continuously decreased both at room temperature and transition temperature along with Curie temperature (322–207 °C). The trend of T_c, $\tan\delta_{RT}$ and $\tan\delta_{Tc}$ were continuously decreasing throughout the series whilst ε_{RT} and ε_{Tc} were maximum at $x=0.6$ and thereafter decreased. In literature, the dielectric permittivity is higher and the diffused phase transition is lesser when PBN is closer to the morphotrophic phase boundary [22]. In our study, we chose the compositions near morphotrophic phase boundary of perovskite PLZT and tungsten bronze PBBN in order to achieve a combined effect of both distinct structures. There has been tremendous study on the synthesis of ferroelectric ceramic materials via high-energy mechanochemical technique [23]. However, there is no literature on the synthesis and characterization of binary structured $(1-x)$PLZT–xPBBiN nanocomposites processed via high-energy mechanical activation technique. It has been reported in the literature that there was no significant difference observed in dielectric properties of PLZT 7/60/40 ceramics with and without excess PbO at higher sintering temperatures [24]. Whereas, in our study the combination of perovskite PLZT and tung-

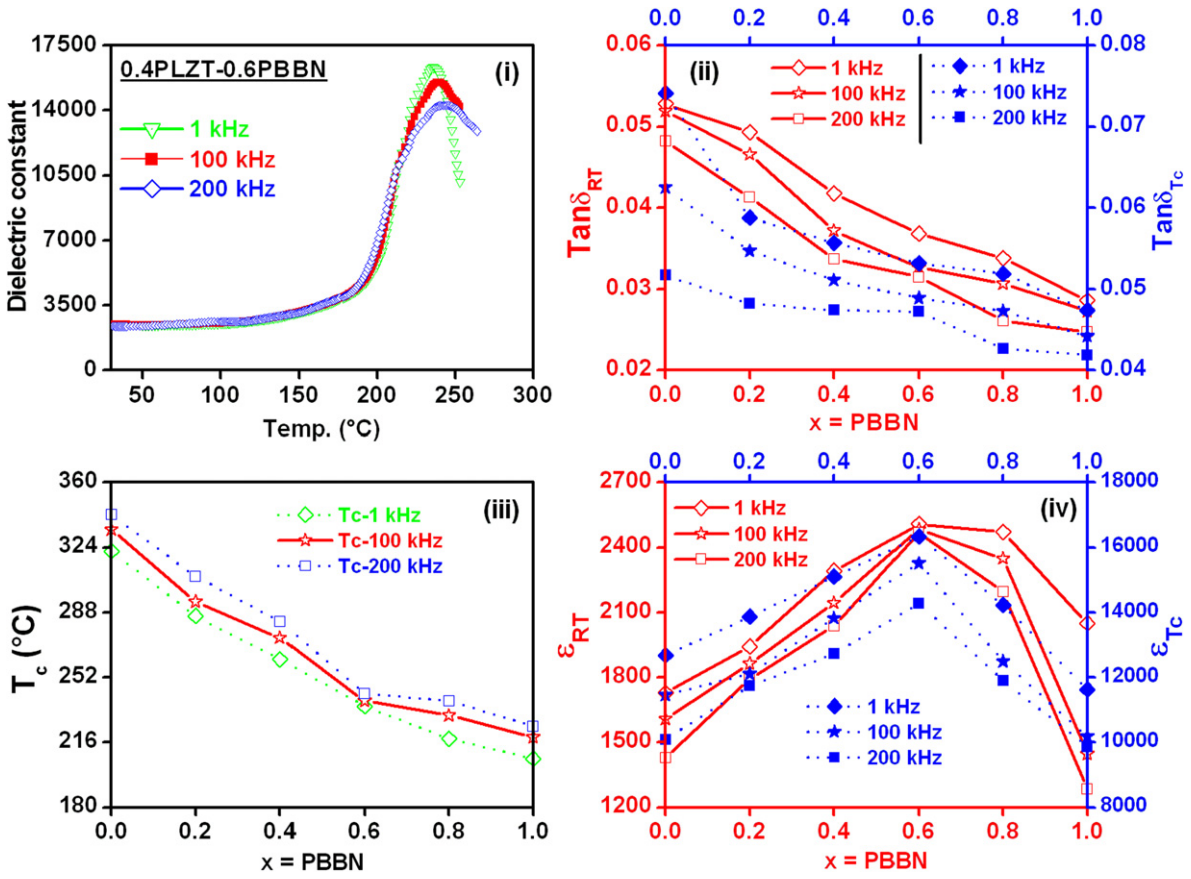

Fig. 5. Dielectric properties of $(1-x)$PLZT–xPBBiN nanoceramic composites.

sten bronze PBBiN resulted in tremendous increase in the dielectric constant.

3.5. Piezoelectric properties of $(1-x)$PLZT–xPBBiN nanocomposites

Fig. 6 depicts piezoelectric properties (piezoelectric charge coefficient, d_{33} and piezoelectric planar coupling coefficient, k_p) of $(1-x)$PLZT–xPBBiN nanoceramic composites. The piezoelectric charge coefficient (d_{33}) and piezoelectric planar coupling coefficient (k_p) exhibited optimum values at $x=0.6$. The dependence

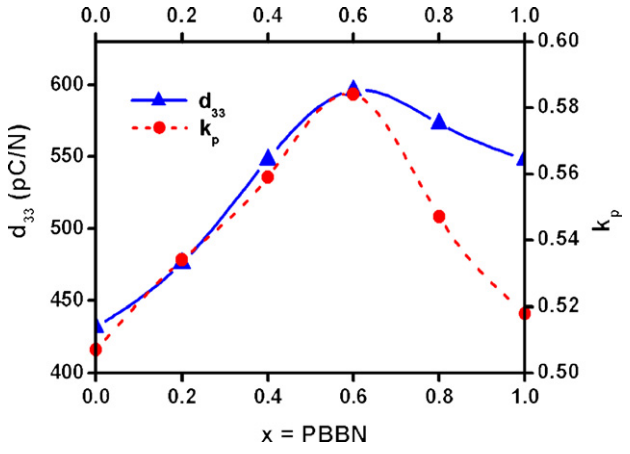

Fig. 6. Piezoelectric properties of $(1-x)$PLZT–xPBBiN nanoceramic composites.

of piezoelectric properties on microstructural evolutions associated with the PLZT perovskite phase in conjunction with tungsten bronze PBBiN phase could have enhanced the domain orientation and thus ionic and electronic polarization. Certainly, denser ceramic composite would have better piezoelectric properties. As a result, high piezoelectric coefficients were achieved in this study. Furthermore, presence of multiple ions of both PLZT and PBBiN in a single ceramic composite influenced the domain orientation and thus, resulted in enhanced piezoelectric properties. The poling process remarkably improved the domain orientation in these dense nanoceramic composites; as a result these composites (PLZT–PBBiN) influenced an electrical response due to a mechanical excitation and a mechanical response due to an electrical excitation. The maximum piezoelectric planar coupling coefficient ($k_p=0.584$) and the piezoelectric charge coefficient ($d_{33}=596$ pC/N) was observed for $x=0.6$ nanoceramic composite. It is reported in literature that the piezoelectric constant for $(K_{0.5}Na_{0.5})_{0.94}Li_{0.06}(Na_{0.94}Sb_{0.06})O_3$ ceramic ($d_{33}=212$ p/CN) and planar electromechanical coupling factor $k_p=46\%$ was the maximum at KNLNS–x/0.06 ceramic [25]. It is well known that the morphotrophic phase boundary (MPB) plays a significant role in the enhancement of functional properties [8]. Generally, the piezoelectric properties of the ceramics are optimal near the MPB region due to the polarization states resulting from coexistence of two phases. A MPB is defined as an abrupt structural change in a solid solution with variation in composition [26]. In our study, we have observed that coexistence of two distinctly structured nanoceramic composite near MPB was optimum at $x=0.6$ which could be ideal for electromechanical and energy harvesting applications.

4. Conclusion

The high-energy mechanical activation milling process was optimized at a speed of 250 rpm for 25 h through Fritsch Pulverisette mill. The nanoceramic composite in which both perovskite and tungsten bronze phases coexisted were successfully prepared in situ. X-ray diffraction studies of $(1-x)$PLZT–xPBBiN indicated a coexistence of perovskite and tungsten bronze phases. The homogenously distributed grains of both perovskite and tungsten bronze confirm well-densified nanoceramic composites. The dielectric constant at room temperature and dielectric maximum at transition temperature were found optimum at $x = 0.6$ at frequencies of 1, 100 and 200 kHz, respectively. The dielectric loss and Curie transition temperature continuously decreased. The optimum piezoelectric planar coupling coefficient ($k_p = 0.584$) and the piezoelectric charge coefficient ($d_{33} = 596$ pC/N) was observed in $x = 0.6$ nanoceramic composite processed through non-conventional synthesis by mechanical activation (MA) technique which could be ideal for electromechanical and energy harvesting applications.

Acknowledgements

This work has been supported by the research grant funded by Fondecyt (Fondo Nacional de Desarrollo Científico y Tecnológico, Chile) through project N°1080635. The authors would like to thank University of Concepcion, Chile and Andhra University, India for their collaboration and support extended. The authors would also like to thank Mr. Ranganathan, Mr. Krishnamurthy and Ms. C.N. Devi for their technical assistance and valuable suggestions extended during this work.

References

[1] C.G. Granquist, Handbook of Inorganic Electronicchromic Materials, Elsevier, Amsterdam, 1995.
[2] S.K. Deb, Phil. Mag. 22 (1973) 801.
[3] E.M. MaCarron, J. Chem. Soc. Chem. Commun. 336 (1986) 501.
[4] R. Guo, A.S. Bhalla, C.A. Randall, Z.P. Chang, L.E. Cross, J. Appl. Phys. 67 (3) (1990) 1453.
[5] C.A. Randall, R. Guo, A.S. Bhalla, L.E. Cross, J. Mater. Res. 6 (1991), 1770.
[6] P.B. Jamieson, S.C. Abrahams, J.L. Bernstein, J. Chem. Phys. 48 (11) (1968) 5048.
[7] P.B. Jamieson, S.C. Abrahams, J.L. Bernstein, J. Chem. Phys. 50 (10) (1969) 4352.
[8] K. Okazaki, K. Nagata, J. Electron. Commun. Soc. Jpn. C53 (1970) 815.
[9] K. Ramam, A.J. Bell, C.R. Bowen, K. Chandramouli, J. Alloys Compd. (2008), doi:10.1016/j.jallcom.2008.05.092.
[10] C.G. Wu, W.L. Lin, Chemistry 57 (1999) 45.
[11] C. Grenthe, M. Sundberg, V.P. Filonenko, I.P. Zibrov, J. Solid State Chem. 168 (1) (2002) 284.
[12] N. Zhang, L. Li, Z. Gui, Mater. Res. Bull. 36 (2001) 2553.
[13] M. Venet, F.L. Zabotto, J.A. Eiras, M. Rincon, P.S. Pizani, D. Garcia, Ferroelectrics 337 (2006) 213.
[14] Y. Xu, Ferroelectric Materials and their Applications, North Holland, Amsterdam, 1991, 110–150.
[15] L.B. Kong, J. Ma, W. Zhu, O.K. Tan, J. Alloys Compd. 322 (2001) 290.
[16] S.E. Lee, J.M. Xue, D.M. Wan, J. Wang, Acta Mater. 47 (9) (1999) 2633.
[17] V.L. Arantes, K.R. Cardoso, D.F.S. Souza, A.A. Silva, G.B. Crochemore, 17° CBECIMat—Congresso Brasileiro de Engenharia e Ciência dos Materiais, Foz do Iguaçu, PR, Brasil, 2006.
[18] Z. Zhou, X. Cheng, P. Du, Mater. Chem. Phys. 100 (2006) 464.
[19] Z.H. Zhou, P.Y. Du, W.J. Weng, G.R. Han, G. Shen, J. Inorg. Mater. 19 (6) (2004) 1322.
[20] A.R. James, J. Subrahmanyam, K.L. Yadav, J. Phys. D: Appl. Phys. 39 (2006) 2259.
[21] M.S. Kim, J.H. Lee, J.J. Kim, H.Y. Lee, S.H. Cho, Ceram. Silikáty 49 (1) (2005) 13.
[22] I.A. Santos, D. Garcia, J.A. Eiras, V.L. Arantes, J. Appl. Phys. 93 (3) (2003) 1701.
[23] L.B. Kong, T.S. Zhang, J. Ma, F. Boey, Prog. Mater. Sci. 53 (2008) 207.
[24] P. Sun, C. Xu, M. Akiyama, T. Watanabe, J. Am. Ceram. Soc. 82 (6) (1999) 1447.
[25] D. Lin, K.W. Kwok, K.H. Lam, H.L.W. Chan, J. Phys. D: Appl. Phys. 40 (2007) 3500.
[26] B. Jaffe, W.R. Cook, H. Jaffe, Piezoelectric Ceramics, Academic Press, New York, 1971, pp. 135–83.